Universiteit Antwerpen

This item is the archived peer-reviewed author-version of:

Sensorless load angle control for energy optimal sinusoidal driven BLDC motor applications

Reference:
De Viaene Jasper, Ceulemans David, Derammelaere Stijn, Stockman Kurt.- Sensorless load angle control for energy optimal sinusoidal driven BLDC motor applications
IEEE/ASME transactions on mechatronics / Institute of Electrical and Electronics Engineers [New York, N.Y.]; American Society of Mechanical Engineers- ISSN 1941-014X - 27:4(2022), p. 2290-2300
Full text (Publisher's DOI): https://doi.org/10.1109/TMECH.2021.3104327
To cite this reference: https://hdl.handle.net/10067/1852130151162165141

uantwerpen.be
Institutional repository IRUA

Sensorless Load Angle Control for Energy Optimal Sinusoidal Driven BLDC Motor Applications

Jasper De Viaene [1,2,3], David Ceulemans [2,3], Stijn Derammelaere [2,3], and Kurt Stockman [1,3]

***Abstract*—Choosing sine-wave instead of square-wave shaped currents to drive a brushless DC (BLDC) motor can increase the energy-efficiency up to 9.5%. But unfortunately for sine-wave setpoint current generation, the typical electronic or sensing low-resolution commutation feedback techniques becomes unavailable. For broad industrial employability, other sensing techniques such as computationally complex observers or signal injection methods requiring access to the switching states of the power electronics are not preferred. This raises the need to develop a computationally sufficiently simple sensorless controller that optimizes the energy efficiency. Therefore, the authors propose a PID algorithm controlling the estimated load angle technique that enables sinusoidal current supply without the need for position feedback or user input. The aim is to implement a controller for dynamic speed-varying BLDC motor applications, which means that accurate speed trajectory tracking behaviour and high robustness against load changes should be guaranteed. The application-dependent PID-settings for setpoint and disturbance rejection control are estimated during an initialization speed trajectory based on only one stator winding current and voltage measurement. The proposed control algorithm is validated through experimental measurements on a BLDC motor with a nominal speed and power of 3000 rpm and 225 W respectively.**

***Index Terms*—brushless dc motor, sensorless control, PID, load angle, system identification, current wave-form**

I. Introduction

Instead of using a mechanical commutator as in the conventional brushed DC motor, Hall sensors embedded in Brushless DC (BLDC) system enable electronic commutation [1]. This makes it a maintenance-free motor because wear due to mechanical friction between the brushes and the commutator, together with electrical erosion, is avoided. On top of that, Hall sensors are inexpensive [2]. Because of these reasons BLDC motors are a suitable candidate for continuous operation applications [3], [4]. BLDC motors are widely found in commercial compressors used in electric vehicles, refrigerators, turbines, fans and pumps [5], [6]. They play a major role in the development of drones in which the energy efficiency is crucial because of the battery supply [7]. Energy efficiency and low cost is especially essential in driving pumps, ventilators and compressors like in white goods. Strict standardization of the power consumption of white goods summarized in the EU energy labelling stimulates companies to develop highly efficient products [8].

[1] Department of Electromechanical, Systems and Metal Engineering, Ghent University campus Kortrijk, Belgium
[2] Department of Electromechanics, Op3Mech, University of Antwerp, Groenenborgerlaan 171, 2020 Antwerp, Belgium
[3] Flanders Make @ UGent - core lab EEDT-MP

On the other hand, embedding the Hall sensors into the stator is a complex process because any misalignment in these Hall sensors with respect to the rotor magnets will generate an error in determination of the rotor position and lead to a lower energy efficiency [9]. A second disadvantage of Hall sensors is their sensitivity to supply voltage peaks [10], which can cause early failure of the Hall sensor and consequently failure of the BLDC motor.

In addition, using Hall sensors detection methods to indicate the commutation moments in BLDC systems enables only square-wave current commutation [11]. However, the literature proves that the torque generation and the overall efficiency is not optimal when driving a BLDC motor with square-wave currents [12], [13]. Several alternative current shape excitation strategies have been developed to further improve the torque generation and energy efficiency of BLDC motors. Many of these algorithms inject current harmonics [12], [14]. These methods require knowledge of the back-EMF harmonic content or motor construction parameters which complicates the general employability.

Therefore, the authors propose a sensorless load angle controller that enables sinusoidal current supply. Only feedback of the load angle which quantifies the efficiency of the torque generation is required. In [15], a load angle estimation method applied to stepping motors is demonstrated. The estimation algorithm only needs one current and one voltage measurement to estimate the back-EMF and subsequently the load angle. The estimation feedback is used to optimize the current level of stepping motors [16]. After these promising results, the load angle estimation and control method are applied to BLDC systems to enable sinusoidal current commutation [17]. Measurements in [17] show an energy saving potential up to 9.5% when the BLDC motor is driven with sinusoidal instead of square-wave shaped currents. With a view to final implementation, the first steps have already been taken for the design-space exploration process for the proposed advanced control technique and its optimal deployment on embedded hardware [18]. However, one missing link still needs to be tackled to arrive at a deployable energy optimal control technology for BLDC motors. Here, in this paper, the aim is to implement a load angle controller for dynamic speed-varying BLDC motor applications, which means that accurate speed trajectory tracking behaviour and high robustness against load changes are given priority.

- The proposed speed control method differs from typical cascaded control as the speed, and current controller are strictly separated. The advantage of this method is that the rotor speed is purely imposed by the current vector

rotational speed which is set by the user, and therefore no speed controller nor position (Hall, encoder, ..) and speed (tacho) sensors are required. The closed-loop load angle PID-controller handles the torque transients by adapting the current amplitude.
- The proposed control techniques enables the more energy-efficient sinusoidal current supply.
- The control approach is challenging as system dynamics are highly non-linear. A linear model is introduced and used to tune an adaptive load angle PID-controller.
- A method is described to estimate the damping and inertia as the optimal PID-settings depend on the mechanical load. These parameters are estimated during an initialization speed trajectory based on the electrical torque equation. In this way, optimal application-specific control is achieved without the need for user input.
- Sensitivity analysis has been carried out showing limited impact of the estimation errors of the system parameters on the robustness of the motor control.
- A feedforward controller is defined which bypasses the controller dynamics and ensures that the machine accurately follows the desired speed trajectory.

The paper is organized as follows. Section II briefly discusses the load angle and torque generation of a BLDC motor. In Section III, the sensorless control strategy to obtain optimal torque generation is proposed. Section IV presents the estimation procedure for the system parameters damping and inertia. Sections V and VI describe the optimized speed trajectory and the current level feedforward. Finally, in Section VIII, the conclusions of the research are formulated.

II. BLDC MOTOR TORQUE GENERATION

Each three-phase BLDC motor configuration regardless of the number of pole pairs or slots can be visualized by the representation in Figure 1(b) if subjected to a few transformations. For example, a BLDC motor with 12 stator slots and 8 rotor poles, as shown in Figure 1(a), has a northern rotor tooth (red) that stands at 45° of a southern rotor tooth (blue) due to the 8 rotor poles. Second, a northern rotor tooth (red) is in line with a southern stator tooth and stands at 30° of the adjacent stator teeth created by the other two phases due to the 12 stator slots. To obtain the simplified representation, the number of pole pairs is taken into account to convert the mechanical angles to electrical angles.

A three-phase voltage source inverter is commonly used to drive a BLDC machine. The sum of the three-phase currents leads to the resulting stator current vector $\mathbf{i}_\mathrm{s}$ depicted in Figure 2. The generated electromagnetic motor torque $\mathbf{T}_\mathrm{em}$ can be expressed as the cross product of the rotor flux linkage space vector $\mathbf{\Psi}_\mathrm{s}$ and the stator current vector $\mathbf{i}_\mathrm{s}$ [19].

$$\mathbf{T}_\mathrm{em} = \mathbf{\Psi}_\mathrm{s} \times \mathbf{i}_\mathrm{s} \tag{1}$$

By neglecting saturation [20], [21], the stator flux linkage space vector $\mathbf{\Psi}_\mathrm{s}$ can be written as the sum of the stator flux linkages, established by the two stator currents in the dq-reference frame fixed to the rotor flux and the permanent

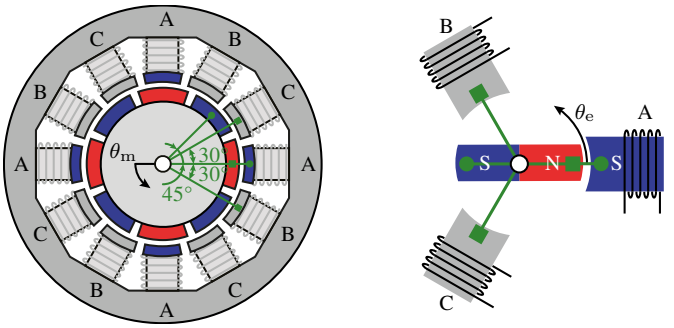

(a) Actual construction (b) Simplified representation

Fig. 1. The actual construction of a BLDC motor with 12 stator slots and 8 rotor poles (a) and the simplified representation of the three-phase BLDC system (b)

magnet rotor flux vector $\mathbf{\Psi}_\mathrm{r}$ as depicted in Figure 2. The electromagnetic motor torque $\mathbf{T}_\mathrm{em}$ can be rewritten as:

$$\mathbf{T}_\mathrm{em} = (\mathbf{\Psi}_\mathrm{r} + L_\mathrm{d}\mathbf{i}_\mathrm{d} + L_\mathrm{q}\mathbf{i}_\mathrm{q}) \times \mathbf{i}_\mathrm{s} \tag{2}$$

Elaboration of the vector products leads to an equation describing the electromagnetic torque as a function of stator current i_s, the rotor flux Ψ_r and the load angle δ, defined as the angle between $\mathbf{i}_\mathrm{s}$ and the rotor flux $\mathbf{\Psi}_\mathrm{r}$:

$$T_\mathrm{em} = \Psi_\mathrm{r}.i_\mathrm{s}.\sin(\delta) + \frac{L_\mathrm{d} - L_\mathrm{q}}{2} i_\mathrm{s}^2.\sin(2\delta) \tag{3}$$

in which the second term represents the reluctance effect which is solely due to the saliency and disappears for a smooth-air-gap machine [20], [21]. By neglecting the reluctance effect, the electromagnetic torque can be written with k_t the torque constant as:

$$\mathbf{T}_\mathrm{em} = \mathbf{\Psi}_\mathrm{r} \times \mathbf{i}_\mathrm{s} \tag{4}$$

$$T_\mathrm{em} = k_\mathrm{t}.|\mathbf{i}_\mathrm{s}|.\sin(\delta) \tag{5}$$

From eq. (5), it can be concluded that maximum torque generation is achieved when the load angle δ is equal to the $\frac{\pi}{2}$ rad. The load angle can thus be seen as a quality factor of the torque generation.

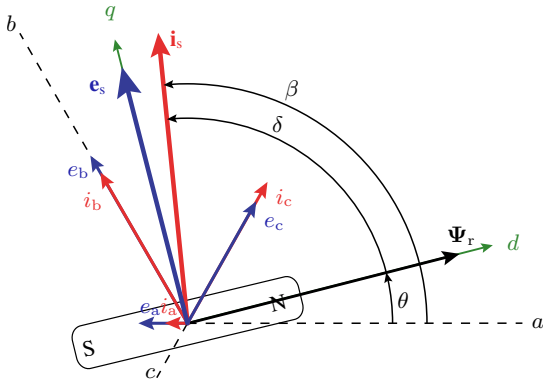

Fig. 2. Vector diagram with stator current $\mathbf{i}_\mathrm{s}$ and stator flux $\mathbf{\Psi}_\mathrm{s}$, rotor flux $\mathbf{\Psi}_\mathrm{r}$ and load angle δ represented in dq-reference frame fixed to the rotor flux

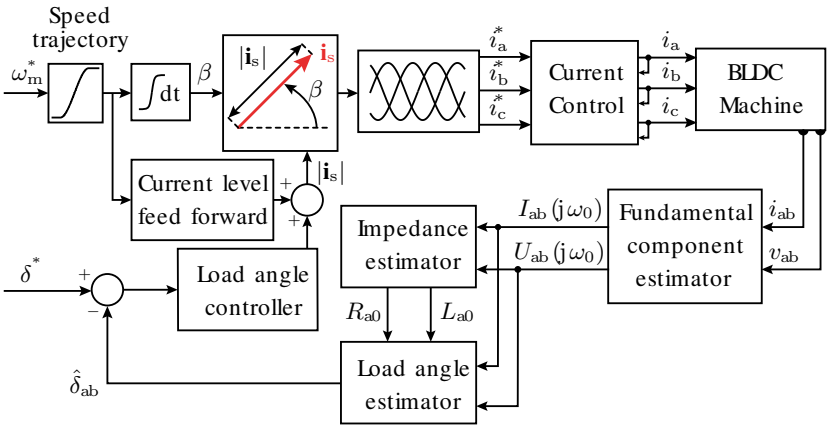

Fig. 3. Proposed sensorless load angle control scheme for BLDC motors, the current level feedforward bypasses the load angle controller and thus directly provides a current level based on the imposed speed

III. Load angle control

The proposed control algorithm for BLDC systems (Figure 3) differs from the typical vector control structure which is characterized by the inner current loop and outer speed loop [22]. The proposed control structure does not contain a speed controller. The speed is imposed in open-loop by a rotating current vector $\mathbf{i}_s$ with angle β. The angle β is calculated by integrating the speed setpoint n^*. In Section V, the speed setpoint procedure is discussed. In this way, the three-phase sinusoidal current setpoints are determined:

$$\begin{aligned} i_a^* &= \frac{2}{3}|\mathbf{i}_s|\cos(\beta) \\ i_b^* &= \frac{2}{3}|\mathbf{i}_s|\cos(\beta - \frac{2\pi}{3}) \\ i_c^* &= \frac{2}{3}|\mathbf{i}_s|\cos(\beta - \frac{4\pi}{3}) \end{aligned} \tag{6}$$

where

$$\beta = \int n^* \mathrm{d}t$$

The sum of the three-phase currents leads to the stator current vector $\mathbf{i}_s$ creating a stator flux $\mathbf{\Psi}_s$ which attracts the rotor flux $\mathbf{\Psi}_r$. As long as the rotor flux lags the current vector by the optimum of $\frac{\pi}{2}$ rad or less the current vector rotational speed purely imposes the rotor speed. If the rotor flux lags the current vector by more than $\frac{\pi}{2}$ rad, the generated motor torque (5) decreases. In that case, synchronization of the fluxes is lost, and the rotor speed drops to zero.

Loss of synchronization should be avoided at all time. Therefore, the load angle estimation is used to observe if the motor follows the imposed acceleration trajectory. However, at lower speeds, the back-EMF is too small to obtain accurate load angle information. Therefore at start-up, closed-loop load angle control is not possible. The controller counters this by applying maximum current at start-up [16].

The advantage of the method, compared to conventional speed control, is that the speed is purely imposed in open-loop and no position and speed feedback is necessary. The disadvantage is that the rotor position and thus back-EMF $\mathbf{e}_s$ is not taken into account to inject the currents to achieve optimal torque generation during start-up. However, to obtain optimal torque generation, the load angle will be controlled to the optimum angle $\frac{\pi}{2}$ by adjusting the current amplitude $|\mathbf{i}_s|$ (5) as soon as information of the load angle is available. Figure 3 shows that the load angle controller reduces the error between the load angle setpoint δ^* and the estimated load angle $\hat{\delta}$ by adjusting the current amplitude $|\mathbf{i}_s|$.

In [23], a BLDC motor simulation model including a hysteresis current control developed for alternative current waveform supply is presented. In [17] this is continued, sinusoidal current waveform measurements are presented and its quality (THDI) and impact on the energy-efficiency are described. Additionally, the load angle estimation technique, based on estimators to determine the fundamental component of the voltage and current measurements to obtain subsequently an estimation of the back-EMF and impedance, is also extensively described in [17]. Measurements show that the load angle can be accurately estimated from a speed of 250 rpm to the rated speed for the motor under test (Table II). All these components of the proposed control scheme are therefore not repeated here. The goal of this paper is to describe the implementation of the load angle controller and the two extensions: current level feed forward and speed trajectory. To obtain optimal load angle control, the controller dynamics need to be adjusted to the system dynamics. This means that in order to achieve a well-considered setting of the controller, it is important to know the system dynamics. For this reason, a process description is given below.

A. System dynamics

As depicted in Figure 3, the magnitude of the stator current vector $\mathbf{i}_s$ is used by the controller to obtain the load angle setpoint. Therefore this section discusses the dynamics of the load angle based on the current level $|\mathbf{i}_s|$ (Figure 4). There is much literature on dynamic BLDC motor models but none that mentions or includes this relationship [24]. Only in [16], the impact of the current level $|\mathbf{i}_s|$ on the load angle δ is described for constant-speed applications. Nevertheless, the behaviour in variable speed applications is not described yet in literature.

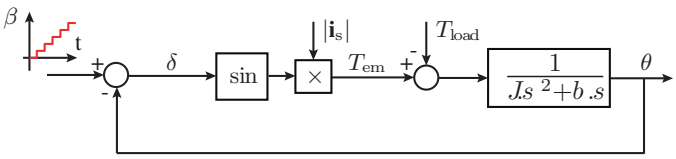

Fig. 4. Description of the dynamic load angle behaviour

The mechanical behaviour of the system can be described in the time domain:

$$T_{\mathrm{em}} - T_{\mathrm{load}} = J\ddot{\theta} + b\dot{\theta} \tag{7}$$

The load is modelled using lumped parameters: inertia J, viscous damping b and a load torque T_{load}. This simplification is permissible as higher-order mechanical systems will often show behaviour that is very similar to that of the second-order systems as in (7) [25].

The motor torque T_{em} in (7) can be represented by the torque equation (5). Substituting (5) in (7) gives:

$$k_{\mathrm{t}}|\mathbf{i}_{\mathrm{s}}|\sin(\delta) - T_{\mathrm{load}} = J\ddot{\theta} + b\dot{\theta} \tag{8}$$

The rotor position θ can be written as the difference between the angular position β of the stator current vector $\mathbf{i}_{\mathrm{s}}$ and the load angle δ where p is the number of pole pairs:

$$k_{\mathrm{t}}|\mathbf{i}_{\mathrm{s}}|\sin(\delta) - T_{\mathrm{load}} = J\left(\frac{\ddot{\beta}}{\mathrm{p}} - \ddot{\delta}\right) + b\left(\frac{\dot{\beta}}{\mathrm{p}} - \dot{\delta}\right) \tag{9}$$

Equation (9) shows a highly non-linear character. To use linear analysis techniques, the electromagnetic torque equation (5) needs to be linearized around the operating point $\left(|\mathbf{i}_{\mathrm{s}}^{'}|, \delta^{'}\right)$:

$$T_{\mathrm{em}} = k_{\mathrm{t}}|\mathbf{i}_{\mathrm{s}}|\sin(\delta) \tag{10}$$

$$T_{\mathrm{em}} = T_{\mathrm{em}}^{'} + \left.\frac{\partial T_{\mathrm{em}}}{\partial|\mathbf{i}_{\mathrm{s}}|}\right|_{(|\mathbf{i}_{\mathrm{s}}^{'}|,\delta^{'})}\left(|\mathbf{i}_{\mathrm{s}}| - |\mathbf{i}_{\mathrm{s}}^{'}|\right) + \left.\frac{\partial T_{\mathrm{em}}}{\partial\delta}\right|_{(|\mathbf{i}_{\mathrm{s}}^{'}|,\delta^{'})}\left(\delta - \delta^{'}\right) \tag{11}$$

$$T_{\mathrm{em}} = k_{\mathrm{t}}\sin(\delta^{'})|\mathbf{i}_{s}| + k_{\mathrm{t}}|\mathbf{i}_{\mathrm{s}}^{'}|.\cos(\delta^{'})\delta - k_{\mathrm{t}}|\mathbf{i}_{\mathrm{s}}^{'}|.\cos(\delta^{'})\delta^{'} \tag{12}$$

This linearization should not lead to errors as the only interest is the dynamic behaviour of the system around the operating point $\left(|\mathbf{i}_{\mathrm{s}}^{'}|, \delta^{'}\right)$. Equation (12) will not be used in predicting motor behaviour for other operating points. Therefore, a description of the linearization error is not given here.

The linearized equation (12) is substituted in (8):

$$k_{\mathrm{t}}\sin(\delta^{'})|\mathbf{i}_{s}| + k_{\mathrm{t}}|\mathbf{i}_{\mathrm{s}}^{'}|\cos(\delta^{'})\delta - k_{\mathrm{t}}|\mathbf{i}_{\mathrm{s}}^{'}|.\cos(\delta^{'})\delta^{'} = T_{\mathrm{load}} + J\frac{\ddot{\beta}}{\mathrm{p}} - J\ddot{\delta} + b\frac{\dot{\beta}}{\mathrm{p}} - b\dot{\delta} \tag{13}$$

The focus is on speed-varying applications through which $\dot{\beta}$ can be replaced by the electrical pulsation ω_{e} or $\frac{\dot{\beta}}{\mathrm{p}}$ can thus be replaced by the mechanical pulsation ω_{m}. After rearrangement this lead to:

$$-k_{\mathrm{t}}\sin(\delta^{'})|\mathbf{i}_{s}| + T_{\mathrm{load}} + J\dot{\omega}_{\mathrm{m}} + b\omega_{\mathrm{m}} + k_{\mathrm{t}}|\mathbf{i}_{\mathrm{s}}^{'}|.\cos(\delta^{'})\delta^{'} = J\ddot{\delta} + b\dot{\delta} + k_{\mathrm{t}}|\mathbf{i}_{\mathrm{s}}^{'}|\cos(\delta^{'})\delta \tag{14}$$

In the Laplace domain this yields:

$$\delta(s) = G_{\mathrm{s}}.|\mathbf{i}_{\mathrm{s}}|(s) + G_{\mathrm{d1}}.T_{\mathrm{load}}(s) + G_{\mathrm{d2}}.\omega_{\mathrm{m}}(s) \tag{15}$$

where

$$G_{\mathrm{s}} = \frac{-k_{\mathrm{t}}\sin(\delta^{'})}{Js^2 + bs + k_{\mathrm{t}}|\mathbf{i}_{\mathrm{s}}^{'}|\cos(\delta^{'})} \tag{16}$$

$$G_{\mathrm{d1}} = \frac{1}{Js^2 + bs + k_{\mathrm{t}}|\mathbf{i}_{\mathrm{s}}^{'}|\cos(\delta^{'})} \tag{17}$$

$$G_{\mathrm{d2}} = \frac{Js + b}{Js^2 + bs + k_{\mathrm{t}}|\mathbf{i}_{\mathrm{s}}^{'}|\cos(\delta^{'})} \tag{18}$$

Based on these functions, a load angle setpoint controller, a load angle disturbance rejection controller and current level feedforward controller are developed in this paper:

- The impact of the current level $|\mathbf{i}_{s}|$ on the load angle δ described by G_{s} (16) will be essential for load angle setpoint control. Based on G_{s}, the load angle controller that adjusts the current level until the load angle is equal to the setpoint load angle δ^{*} will be designed (Section III-B1).
- A change in load torque is considered as a disturbance factor. This disturbance behaviour on the load angle is described by G_{d1} (17) and needs to be eliminated by the load angle disturbance rejection controller as fast as possible, see Section III-B2.
- A speed variation can also be seen as a disturbance. However, here the speed is directly imposed by the user and thus always known. Therefore, a current level feedforward controller can be designed that anticipates on speed variations based on G_{d2} (18), see Section VI.

The process dynamics of the system are characterized by the location of the poles being the roots of the denominator of (16-18). The characteristic equation that describes the location of these poles can be written as:

$$s^2 + \frac{b}{J}s + \frac{k_{\mathrm{t}}}{J}|\mathbf{i}_{\mathrm{s}}^{'}|\cos(\delta^{'}) = 0 \tag{19}$$

As can be deduced from (19), the behaviour depends on the mechanical parameters of the system. Besides the poles, also zeros influence the process dynamics. Only function G_{d2} describing the impact of the speed on the load angle contains a zero. This zero has to be taken into account during the design of the current level feedforward controller.

On the assumption that the system is not over-damped (high damping b), the poles of the system are:

$$a_{1,2} = -\frac{b}{2J} \pm \mathrm{j}\sqrt{\left|\frac{b^2}{4.J^2} - \frac{k_{\mathrm{t}}|\mathbf{i}_{\mathrm{s}}^{'}|\cos(\delta^{'})}{J}\right|} \tag{20}$$

The system poles a_1 and a_2 are complex conjugates. The negative real part of the poles indicates the system is stable. The complex part introduces the non-desired oscillating behaviour of the system during transients.

B. Adaptive load angle PID-controller

The load angle controller that adjusts the load angle by adapting the current level should prevent oscillating load angle behaviour. In the optimal case, the load angle controller completely cancels the system poles a_1 and a_2 to eliminate all oscillating behaviour of the system. The main reason for this choice is that the critical load angle limit of $\delta = \frac{\pi}{2}$ rad may not be exceeded at all time.

The transfer function of the system (16) can be represented by a system with K_s the system gain and a_1 and a_2 the system poles:

$$G_\mathrm{s} = \frac{K_\mathrm{s}}{(s-a_1).(s-a_2)} \tag{21}$$

A rule of thumb is that high-end control methods should only be considered if a PI or PID-controller does not lead to the desired result. The PI and PID-controller have to act on load angle error $\Delta\delta$ by adjusting the current level $|\mathbf{i}_\mathrm{s}|$. A PI-controller introduces only one zero. This means, a PI-controller can only compensate for the real part of the system poles. A PID-controller adds two zeros. PID-controller that already includes a first-order filter with time constant τ_d required for flawless D-action can be written in the s-domain as:

$$\begin{aligned} G_{\mathrm{c-PID}} &= K_\mathrm{p}\left(\frac{1}{T_\mathrm{i}}.\frac{1}{s} + \frac{T_\mathrm{d}.s}{\tau_d.s+1} + 1\right) \\ &\approx K_\mathrm{p}.\left(\frac{T_\mathrm{d}.s^2 + s + \frac{1}{T_\mathrm{i}}}{s}\right) \end{aligned} \tag{22}$$

This means, a PID-controller is also able to compensate for the imaginary part of the system poles. The D-action adds the necessary damping in the control loop to avoid load angle overshoot. This clarifies the choice for a PID-controller in this study.

The transfer function of a PID-controller can be written as follows if the filter for D-action is neglected:

$$G'_{\mathrm{c-PID}} = K_\mathrm{p}.\frac{(s-a_1).(s-a_2)}{s} \tag{23}$$

The complete open-loop transfer function is then:

$$\begin{aligned} G_\mathrm{OL} &= \frac{K_\mathrm{s}}{(s-a_1).(s-a_2)}.K_\mathrm{p}.\frac{(s-a_1).(s-a_2)}{s} \\ &= \frac{K_\mathrm{s}.K_\mathrm{p}}{s} \end{aligned} \tag{24}$$

The resulting closed-loop transfer function is:

$$G_\mathrm{CL} = \frac{1}{\frac{1}{K_\mathrm{s}.K_\mathrm{p}}.s+1} \tag{25}$$

In other words, when using the controller proposed in (23), the closed-loop system is reduced to a first order system. To obtain this, the zeros of the PID controller in (22) have to cancel the poles of system (16). If the first-order filter with time constant τ_d is neglected (τ_d=0), the integrator gain T_i and the differentiator gain T_d of the PID-controller can then be determined:

$$T_\mathrm{i} = \frac{b}{k_\mathrm{t}|\mathbf{i}'_\mathrm{s}|\cos(\delta')} \tag{26}$$

$$T_\mathrm{d} = \frac{J}{b} \tag{27}$$

The previous equations show that to determine the control parameters, the torque constant k_t, damping b, inertia J and the operating load angle δ' which is equal to the estimated load angle $\hat{\delta}$ have to be known. The latter dependency means that the PID-parameters needs to be continuously updated which results in an adaptive controller. This dependency is a serious disadvantage of the controller. But if optimal control is the goal, these parameters must be known or estimated [26], [12], [27]. In Section IV, a method is developed to estimate the friction $\hat{b}$ and inertia $\hat{J}$.

The only design parameter of the PID-controller that remains undetermined is the proportional gain K_p. The setting of this parameter depends on the task assigned to the controller. Should the controller follow setpoint changes or should the controller eliminate disturbances as fast as possible? Therefore, in the following sections, a distinction is made between setpoint control and disturbance rejection control.

A drawback of the presented PID-controller is that the settings depend on the system parameters. Of course, there are already simpler PID-tuning methods defined in literature such as "Probably the best simple PID tuning rules in the world" [28]. Nevertheless, in [28], the proposed methods also require knowledge of the process time constants for proper operation. Other control principles such as Model Reference Adaptive Control (MRAC) [29] do not require system knowledge but determine in an iterative way the controller settings based on the error between the setpoint and the actual value. The proposed control principle does not need to wait for errors to correct the control settings as during this process the load angle may exceed the critical limit, which would greatly reduce overall operating stability.

1) Load angle setpoint control: In the optimal case, the current level will be optimized as quickly as possible without any overshoot on the load angle. Avoiding overshoot allows the load angle setpoint δ^* to be set closer to the critical limit of $\frac{\pi}{2}$.

To determine K_p of the PID-controller for setpoint control, the resulting open-loop transfer is defined without neglecting the filter time constant τ_d of the D-action. The delay on the load angle feedback introduced by the load angle estimator should also be taken into account [15]. This delay is described here as dead time t_d is equal to:

$$t_\mathrm{d} = \frac{1}{2\mathrm{p}\omega_m} \tag{28}$$

This dead time t_d is depending on the mechanical motor speed ω_m. The resulting open-loop transfer is then equal to:

$$\begin{aligned} G_\mathrm{OL} &= \frac{K_\mathrm{s}K_\mathrm{p}}{s}\frac{1}{\tau_d.s+1}\mathrm{e}^{-\frac{1}{2\mathrm{p}\omega_m}s} \\ &= \frac{K_\mathrm{s}K_\mathrm{p}/\tau_\mathrm{d}}{(s+\frac{1}{\tau_\mathrm{d}})s}\mathrm{e}^{-\frac{1}{2\mathrm{p}\omega_m}s} \end{aligned} \tag{29}$$

The proportional gain K_p of the controller should be tuned so that fast response is obtained without overshoot on the load angle. Therefore, a critically damped system is desired which means that the relative damping of the closed-loop ζ_cl must be equal to 1. The relative damping ζ_cl of the closed-loop system can be related to the phase margin ϕ_PM of the open-loop frequency response (29) [30]:

$$\phi_\mathrm{PM} = \tan^{-1}\left(\frac{2\zeta_\mathrm{cl}}{\sqrt{-2\zeta_\mathrm{cl}^2+\sqrt{1+4\zeta_\mathrm{cl}^4}}}\right) \quad (30)$$

$$\overset{\zeta_\mathrm{cl}=1}{=} 76° \quad (31)$$

To obtain a 76° phase margin ϕ_PM, the open-loop phase ϕ_OL should be equal to -104° at the bandwidth with frequency ω=ω_{PM} for which $|G_\mathrm{OL}|$=0 dB. To realize this, first, the open-loop phase ϕ_OL and gain $|G_\mathrm{OL}|$ are deduced from (29):

$$\phi_\mathrm{OL} = -\tan^{-1}(\tau_\mathrm{d}\omega) - \frac{\pi}{2}\ \mathrm{rad} - \frac{1}{2\mathrm{p}\omega_m}\omega \quad (32)$$

$$|G_\mathrm{OL}| = \frac{K_\mathrm{s}K_\mathrm{p}}{\tau_\mathrm{d}\omega\sqrt{\omega^2+\frac{1}{\tau_\mathrm{d}^2}}} \quad (33)$$

Equation (32) is not directly solvable to ω in a simple way. To avoid a look-up table with several solution for ω as a function of the phase ϕ_OL, the motor speed ω_m and the filter constant τ_d, it is preferred to obtain a solution via an iterative solver. For this problem Newton's Gradient based optimization technique is used [31]. A solution for ω_PM is calculated in an iterative way at each time instance t_k as follows with Q, the objective function and $\frac{\mathrm{d}Q}{\mathrm{d}\omega_\mathrm{PM}}$, its derivative to the pulsation ω_PM:

$$\omega_\mathrm{PM}(t_{\mathrm{k}+1}) = \omega_\mathrm{PM}(t_\mathrm{k}) - \frac{\mathrm{d}Q}{\mathrm{d}\omega_\mathrm{PM}}(t_\mathrm{k}) \setminus Q(t_\mathrm{k}) \quad (34)$$

with

$$Q(t_\mathrm{k}) = -\tan^{-1}\left(\tau_\mathrm{d}\omega_\mathrm{PM}(t_\mathrm{k})\right) - \frac{\pi}{2}\mathrm{rad} - \frac{1}{2\mathrm{p}\omega_m}\omega_\mathrm{PM}(t_\mathrm{k}) + \pi - \phi_\mathrm{PM}$$

$$\frac{\mathrm{d}Q}{\mathrm{d}\omega_\mathrm{PM}}(t_\mathrm{k}) = \frac{-\tau_\mathrm{d}}{1+\tau_\mathrm{d}^2\omega_\mathrm{PM}(t_\mathrm{k})^2} - \frac{1}{2\mathrm{p}\omega_m}$$

In this way, the required bandwidth ω_PM of the controller can be calculated and continuously updated. After limited number of iterations, a solution for ω_PM is found based on (34) with an error smaller then 0.1 $\mathrm{rad\,s^{-1}}$. Finally, the proportional gain K_p of the PID-controller can be defined based on (33):

$$K_\mathrm{p} = \frac{\tau_\mathrm{d}\omega_\mathrm{PM}\sqrt{\omega_\mathrm{PM}^2+\frac{1}{\tau_\mathrm{d}^2}}}{K_\mathrm{s}} = -\frac{J\tau_\mathrm{d}\omega_\mathrm{PM}\sqrt{\omega_\mathrm{PM}^2+\frac{1}{\tau_\mathrm{d}^2}}}{k_\mathrm{t}\sin(\delta')} \quad (35)$$

Figure 5 shows simulation results of the behaviour of the load angle controller using the complete motor model when the starting nominal current level is 13.9 A and the load angle setpoint δ^* is 1.2 rad for a K_p of the PID-controller set to half, equal to or twice the calculated value based on (35).

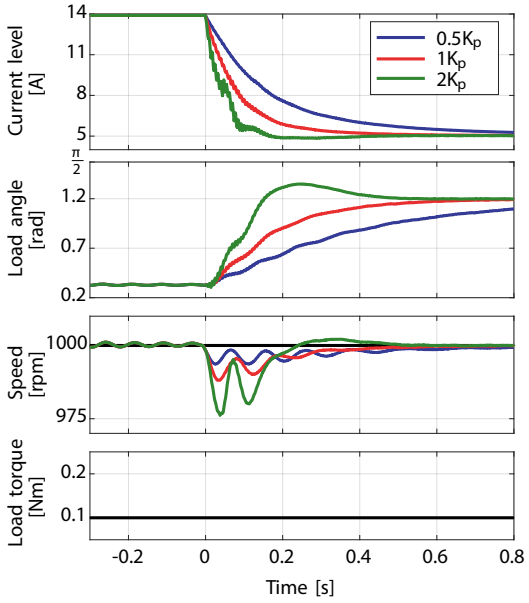

Fig. 5. Simulation results of the behaviour of the load angle controller when the starting current level is 13.9 A and the load angle setpoint δ^* is 1.2 rad for a K_p of the PID-controller set to half, equal to or twice the calculated value based on (35)

When K_p is set too high, the closed-loop system is under-critically damped, which results in an overshoot of the load angle. When K_p is set too low, the closed-loop system is over-critically damped, which results in a slower response of the load angle controller.

2) Load angle disturbance rejection control : To reject load angle disturbances due to changes in speed or load torque, the phase margin ϕ_PM should be as small as possible so that the controller bandwidth ω_PM is as high as possible to reject high frequency disturbances [32]. A trade-off must be made between the dynamics and the stability of the controller to set the phase margin ϕ_PM. Thereafter, the controller bandwidth ω_PM and proportional gain K_p can again be determined in the same way by means of (34) and (35).

Figure 6 shows a simulation result of the behaviour of the closed-loop during a load torque disturbance of 0.1 Nm when the load angle setpoint δ^* is 1.2 rad for a phase margin ϕ_PM equal to 0°, 10° and 20°. If the phase margin is set too low (ϕ_PM = 0°), the controller is too aggressive and the output of the controller may run into the current level limits. With such a setting the transient can best be suppressed, but in practice such a setting will never be applied. If the phase margin ϕ_PM is set too high, the load angle controller becomes slower and disturbances are slowly rejected. In this example, the load angle increases to a value of 1.42 rad if the phase margin ϕ_PM is set to 20°. These results show that a phase margin ϕ_PM of 10° is better as the load angle only increases to a value of 1.36 rad and stable operation is guaranteed.

The inertia J and damping b of the application turn out to be 2.5e-4 $\mathrm{kg\,m^2}$ and 3.3e-4 $\mathrm{N\,m\,s\,rad^{-1}}$.

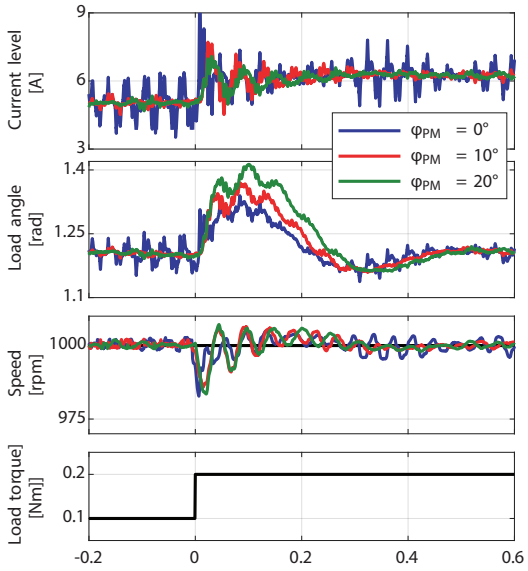

Fig. 6. Simulation results of the behaviour of the load angle controller during a load torque disturbance of 0.1 Nm when the load angle setpoint δ^* is 1.2 rad for a phase margin ϕ_{PM} equal to 0°, 10° and 20°

IV. Estimation of the Mechanical Parameters

In Section III-B, an adaptive PID-controller is preferred for optimizing the current level $|\mathbf{i}_\mathrm{s}|$ based on feedback of the estimated load angle $\hat{\delta}$. Disadvantageous is that the optimal proportional gain K_p, integration time T_i and differential time T_d are dependent on the total inertia J and damping b of the system.

One option seems to estimate the damping $\hat{b}$ at constant speed because then the acceleration torque is zero and thus the effect of the inertia is excluded. The damping $\hat{b}$ is supposed to be speed-independent:

$$T_\mathrm{em} = \hat{b}.\omega_m + T_\mathrm{load} \tag{36}$$

It is not an option to determine these parameters based on instantaneous values as the motor torque can oscillate heavily. Therefore each term in (36) is integrated over a specified time to obtain an average trend. This procedure is carried out at two different speed levels (ω_1 and ω_2) so that two equations are obtained:

$$\int_{t_1}^{t_2} T_{\mathrm{em}_1} = \hat{b}.\int_{t_1}^{t_2} \omega_1 + \int_{t_1}^{t_2} T_\mathrm{load} \tag{37}$$

$$\int_{t_4}^{t_5} T_{\mathrm{em}_2} = \hat{b}.\int_{t_4}^{t_5} \omega_2 + \int_{t_4}^{t_5} T_\mathrm{load} \tag{38}$$

These equations can be used to determine the two unknowns, being the damping $\hat{b}$ and the load torque T_load.

As the only parameter of interest is the damping $\hat{b}$, the load torque T_load can be eliminated by subtracting (37) by (38). The damping $\hat{b}$ can then be estimated as:

$$\hat{b} = \frac{\int_{t_1}^{t_2} T_{\mathrm{em}_1} - \int_{t_4}^{t_5} T_{\mathrm{em}_2}}{\int_{t_1}^{t_2} \omega_1 - \int_{t_4}^{t_5} \omega_2} \tag{39}$$

The only condition for achieving a correct result is that during both integration periods, the size and behaviour of the load torque are the same. To estimate the inertia $\hat{J}$, equation (7) is retaken:

$$T_\mathrm{em} = \hat{J}.\alpha_\mathrm{m} + \hat{b}.\omega_m + T_\mathrm{load} \tag{40}$$

Again, each term in (40) is integrated over a specified time to obtain an average trend. This procedure is carried out two times for an acceleration and deceleration level with the same magnitude (α_1 and $-\alpha_1$), as is illustrated in Figure 7 by the red time periods. Two equations are obtained:

$$\int_{t_2}^{t_3} T_{\mathrm{em}_1} = -\hat{J}\int_{t_2}^{t_3} \alpha_1 + \hat{b}\int_{t_2}^{t_3} \omega_{1:2} + \int_{t_2}^{t_3} T_\mathrm{load} \tag{41}$$

$$\int_{t_5}^{t_6} T_{\mathrm{em}_2} = \hat{J}\int_{t_5}^{t_6} \alpha_1 + \hat{b}\int_{t_5}^{t_6} \omega_{1:2} + \int_{t_5}^{t_6} T_\mathrm{load} \tag{42}$$

The acceleration and deceleration levels should be chosen in the same order of magnitude as this is necessary to ensure that damping $\hat{b}$ inaccuracies do not affect the estimation of inertia $\hat{J}$. By doing this, the friction torque generated by the damping $\hat{b}$ and the load torque T_load can be eliminated by subtracting (41) by (42). As a result, the problem of estimating damping $\hat{b}$ and inertia $\hat{J}$ has been decoupled. The inertia $\hat{J}$ can then be calculated as follow:

$$\hat{J} = \frac{\int_{t_5}^{t_6} T_{\mathrm{em}_2} - \int_{t_2}^{t_3} T_{\mathrm{em}_1}}{\int_{t_5}^{t_6} \alpha_{m_1} - \int_{t_2}^{t_3} -\alpha_{m_1}} \tag{43}$$

$$= \frac{\int_{t_5}^{t_6} T_{\mathrm{em}_2} - \int_{t_2}^{t_3} T_{\mathrm{em}_1}}{2\int_{t_5}^{t_6} \alpha_{m_1}} \tag{44}$$

Figure 7 shows the imposed speed and acceleration profile during which the damping and inertia of the system are estimated. The time intervals depicted in green show the moments when the damping $\hat{b}$ is estimated. The time intervals depicted in the red show when the estimation of the inertia $\hat{J}$ is performed. This procedure is executed at the maximum current level to prevent that the load angle exceeds its critical value.

Table I gives an overview of the average estimation and error of the damping $\hat{b}$ and inertia $\hat{J}$ over 10 measurements and this for different speed n, load torque T_load and current levels $|\mathbf{i}_\mathrm{s}|$. The error on the estimation of damping $\hat{b}$ and inertia $\hat{J}$ is maximum 19% and 9% respectively, even after averaging over 10 estimation procedures. The biggest errors occur at low motor load. This is because the acceleration torque is less

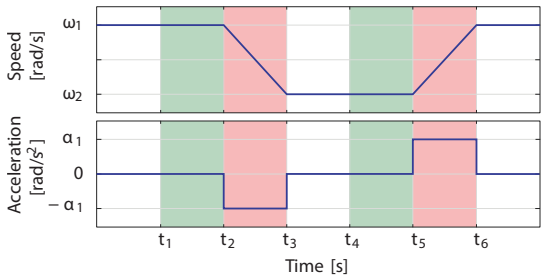

Fig. 7. Imposed speed and acceleration profile for estimating the inertia during the red zone and estimating the damping during the green zone

TABLE I
THE AVERAGE AND STANDARD DEVIATION OVER 10 MEASUREMENTS OF THE ESTIMATED INERTIA AND DAMPING DEDUCTED ON THE BLDC MOTOR FOR DIFFERENT SPEED, LOAD TORQUE AND CURRENT LEVELS

Speed n [rpm]	Load T_{load} [Nm]	Current $\lvert\mathbf{i}_\text{s}\rvert$ [A]	Damping $\hat{b}$ [10^{-4} N m s rad^{-1}]	Inertia $\hat{J}$ [10^{-4} kg m]
1000	0.2	13.7	2.51 ± 0.32	2.55 ± 0.15
1000	0.4	13.7	2.54 ± 0.28	2.32 ± 0.13
2000	0.2	13.7	2.96 ± 0.33	2.54 ± 0.09
2000	0.4	13.7	3.11 ± 0.38	2.24 ± 0.08
1000	0.2	8	2.61 ± 0.24	2.46 ± 0.07
2000	0.2	8	2.86 ± 0.25	2.43 ± 0.07

significant compared to the average torque during the speed transients at low motor load. In Section VII, the impact of these significant estimation errors of damping and inertia on the motor control will be evaluated. For the damping, it can be concluded that the estimation error is smaller if the procedure is executed at higher motor speed. The reason for this is that the proportion of motor torque that goes into overcoming the damping is greater at higher speeds.

V. Optimized Speed Trajectory

In Section III-B2, only a torque change is discussed as a disturbance error. A speed change can also be classified as a disturbance factor. However, the speed ω_m is purely imposed by the user. The mechanical speed ω_m can thus be seen as a disturbance factor known in advance. This gives the freedom to impose well-chosen speed trajectories. In this section, the way a speed trajectory is imposed is explained.

From the derivation of the relation between the load angle δ and the imposed speed ω_m (18), it can be concluded that a step speed change is not a good option as the load angle is related by a transfer function with $Js+b$ in the numerator. This means that the load angle δ sharply increases at high acceleration trajectories. Linear acceleration profiles are a solution to the problem but are not optimal as the begin, and endpoint of the trajectory are not optimized and can thus result in a high jerk.

Therefore, in this research, it is proposed to apply a point-to-point (PTP) trajectory which is described by a sixth-degree polynomial, which satisfies the end conditions of zero acceleration and jerk at the initial and final times [33]. This type of speed control will also benefit the drive efficiency during startup and speed setpoint changes [34].

VI. Current Level Feedforward

A positive effect of the identification of the system parameters damping $\hat{b}$ and inertia $\hat{J}$ in Section IV is the fact that the necessary driving torque can be determined directly based on the setpoint. This information is very beneficial to program a feedforward controller which bypasses the controller dynamics and ensures that the machine accurately follows the desired setpoint [35].

Equipped with current level feedforward as in Figure 3, the total controller (load angle + feedforward controller) can immediately anticipate to speed setpoint changes without waiting for an error on the actual load angle created by the speed change. In this way, the current level feedforward can support the load angle controller so that the load angle can be kept more constant during speed transients. This ensures that the optimized speed trajectory will be tracked as good as possible. The current level feedforward level is calculated based on the imposed speed ω_m, torque constant k_t, and the mechanical inertia J and damping b. Based on the torque equation (8), the necessary current level can be directly calculated:

$$|\mathbf{i}_\text{s}| = \frac{J\dot{\omega}_\text{m} + b\omega_\text{m}}{k_\text{t}\sin(\delta)} \tag{45}$$

Figure 8 shows the final measurement result of the load angle controller enabling sinusoidal current supply for BLDC motor. The control method imposes the nominal current level at start-up. Thereafter, the current level is reduced to a level related to the motor power required to drive the load based on feedback of the load angle. The proposed control method for BLDC motor works in both cases, partial and full load. However, at and closed to the rated operating conditions, small current level adaptions are only possible. Through this, the authors prefer to show measurements performed at average speed and load torque were preferred by the authors. The setpoint load angle δ^* is set to 70° and a phase margin ϕ_PM of 10° is preferred for stability reasons. Prior to the experiment, the estimation procedure for estimating mechanical parameters is performed. The damping $\hat{b}$ and inertia $\hat{J}$ are estimated to be 2.82e-4 N m s rad^{-1} and 2.52e-4 kg m, respectively. Based

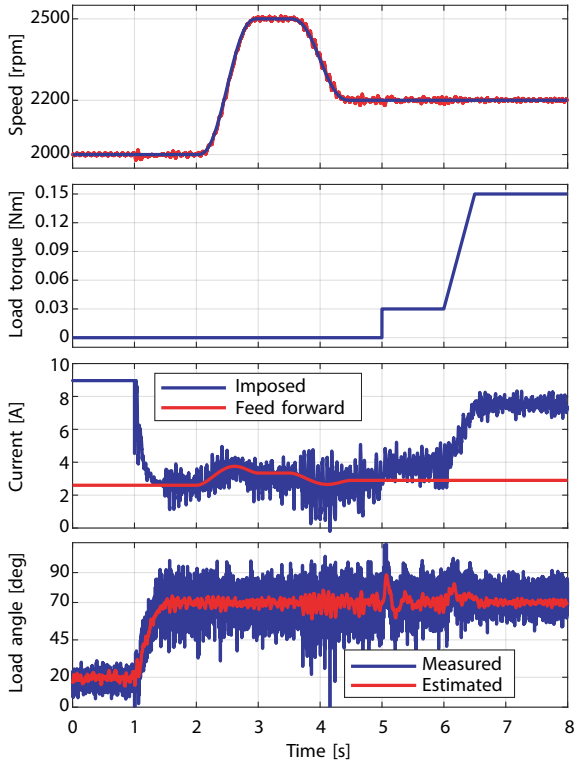

Fig. 8. Measurement result of the behaviour of the load angle controller during speed and load torques changes for a load angle setpoint δ^* = 70°

on (26-27,35), K_p, T_i and T_d are set to 0.35 $\mathrm{A\,rad^{-1}}$, 0.036 s and 0.89 s at the beginning of the experiment. Since K_p and T_i depend on the load angle, these parameters change during the experiment. K_p and T_i increase and decrease respectively as the load angle setpoint is reached. At time instance 2 s, the speed is increased from 2000 to 2500 rpm using the speed trajectory as described in Section V. After that, the speed is reduced to 2200 rpm. During this speed trajectory, the necessary current level is calculated. This helps the load angle controller to maintain the load angle constant within a margin of $\pm$ 5°. At time instance 5 s and 6 s, a step load torque disturbance and linear increasing load torque disturbance are respectively imposed to the BLDC motor. During these transients, the current feedforward cannot anticipate, and a load angle error must first occur before the controller can react to it. A step load torque is, of course, an extreme disturbance, which means that some overshooting of the load angle cannot be avoided. In this situation for a torque jump of 0.03 Nm, the overshoot on the load angle above the load angle setpoint δ^* is limited to 26° and completely eliminated after 0.55 s. During the linear increase of the load torque from 0.03 Nm to 0.15 Nm, the maximum load angle is equal to 81° and is then systematically reduced.

One remark is that the previous measurements are carried out assuming that the damping $\hat{b}$ and inertia $\hat{J}$ are exactly known. In the next section, the impact of damping and inertia estimation errors on the load angle control is examined.

VII. Impact of the Estimation Error of the Damping and Inertia on Motor Control

Setting the proportional action K_p of the load angle PID-controller as described above results in a controlled system as fast as possible without overshoot on the load angle. This is the case if the mechanical system parameters are perfectly known. However, estimation errors can be due to the inaccuracy of the estimation procedure but also due to modification of the actual mechanical parameters. It is assumed that the mechanical parameters are constant during the process. If this is not the case, then the estimation procedure must be carried out frequently and the time instances (Figure 7) must be adapted to the varying load profile.

Figures 9 shows the impact for a number of incorrect estimation values of the inertia $\hat{J}$ on the motor control if the same speed and load torque transients are imposed as in Figure 8. When the inertia $\hat{J}$ is set too high with respect to the real inertia J, the proportional gain K_p (35) and the derivative factor T_d (27) of the PID-controller are set higher. Figure 9(b) shows that when the inertia is set to 130%, the overshoot on the load angle during the step load torque disturbance is even reduced from 86° to 79°. However, when the inertia $\hat{J}$ is 140% of the actual inertia J, the open-loop phase margin decreases from 40° to 0° and results thus in an unstable closed-loop system, see Figure 9(a). When the inertia $\hat{J}$ is lower than the actual inertia J, the proportional gain K_p (35) and the derivative factor T_d (27) of the PID-controller are set lower. This controller is slower resulting in overshoot on the load angle during torque transients.

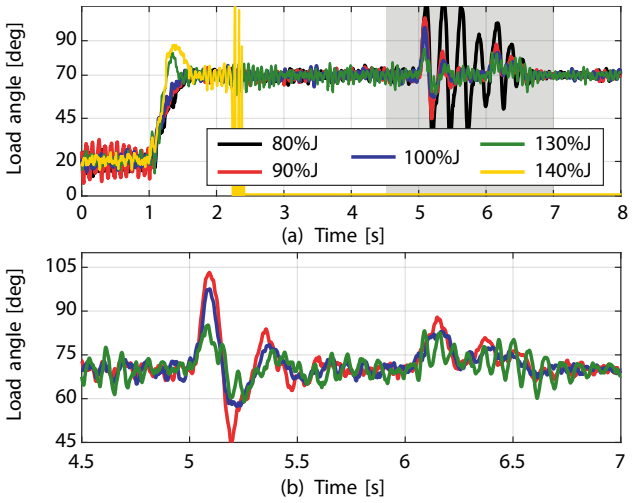

Fig. 9. Measurement result of the impact for a number of incorrect estimations of the inertia $\hat{J}$ on the load angle during a speed and load torques changes as in Figure 8 (a) and detailed view for the three stable situations of the load angle during the torque transient (b)

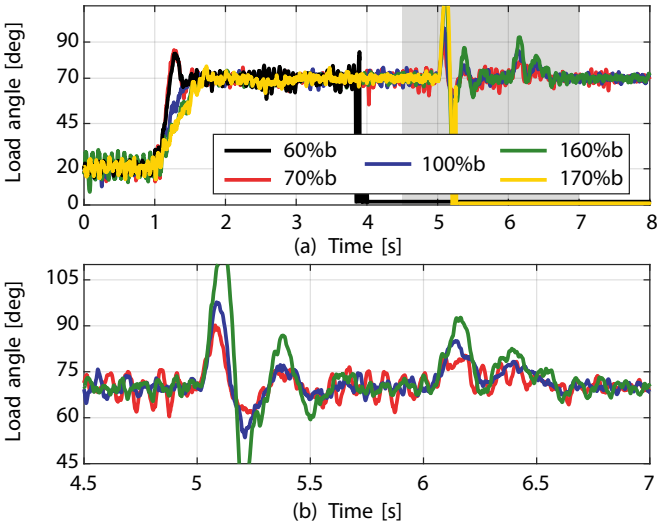

Fig. 10. Measurement result of the impact for a number of incorrect estimations of the damping $\hat{b}$ on the load angle during a speed and load torques changes as in Figure 8 and Figure 9 (a) and detailed view for the three stable situations of the load angle during the torque transient (b)

Figure 10 shows the impact of incorrect estimation of the damping $\hat{b}$ on the motor control for the same speed and load torque transients. When the damping $\hat{b}$ is set too high with respect to the actual damping b, this results in a slower system through which the overshoot on the load angle during torque transients becomes bigger and may result in instability (170% of damping b). When the damping $\hat{b}$ is estimated too low with respect to the real damping b, this results in a faster system and thus less overshoot on the load angle, (Figure 10(b)). However, when the damping is 60% lower then the real damping, the phase margin ϕ_PM decreases to 0° and the closed-loop system becomes again unstable.

The measurements show that the proposed motor control technique can cope with estimation errors on inertia and

damping. However, the error on inertia and damping must be limited within the range of [90%,130%] and [70%,160%] of the actual values. Table I showed the estimation errors were within a range of [93%,102%] and [81%,100.1%] for the specific trajectory.

VIII. Conclusion

Literature shows an energy saving potential when the BLDC motor is driven with sinusoidal instead of square-wave shaped currents. But unfortunately for sine-wave setpoint current generation, the typical electronic low-resolution commutation feedback techniques becomes unavailable. Techniques such as Hall sensors or sensorless algorithms based on back-electromotive force (back-EMF) sensing to detect rotor position information are inadequate for sinusoidal current generation. The proposed speed control method enables the more energy-efficient sinusoidal current supply through which it differs totally from typical cascaded control as the speed, and current controller are strictly separated. The advantage of this method is that the rotor speed is purely imposed by the current vector rotational speed which is set by the user, and therefore no speed controller nor position (Hall, encoder) and speed (tacho) sensors are required. The closed-loop load angle PID-controller handles the torque transients by adapting the current amplitude.

The control approach is challenging as system dynamics are highly non-linear. A linear model is introduced and used to tune an adaptive load angle PID-controller. A method is described to estimate the damping and inertia as the optimal PID-settings depend on the mechanical load. These parameters are estimated during an initialization speed trajectory based on the electrical torque equation. In this way, optimal application-specific control is achieved without the need for user input. Sensitivity analysis has been carried out showing limited impact of the estimation errors of the system parameters on the robustness of the motor control. A positive effect of the identification of the system parameters is the fact that the necessary driving torque can be calculated directly during motor operation based on the imposed motor speed. This information is very beneficial to program a feed forward controller which bypasses the load angle controller dynamics and ensures that the machine accurately follows the desired speed trajectories. To finalize this research work, the control technique should be validated on an existing industrial application with an challenging speed and load torque profile.

Acknowledgment

Research funded by a PhD grant of the Research Foundation Flanders (FWO), Belgium.

References

[1] R. Rabinovici, "Back-EMF waveforms and core losses in brushless DC motors," vol. 141, no. 3, 1994.

[2] Y. Zhao, W. Huang, and J. Yang, "Fault diagnosis of low-cost Hall-effect sensors used in controlling permanent magnet synchronous motor," *19th International Conference on Electrical Machines and Systems (ICEMS)*, no. 1, pp. 2–6, 2016.

[3] K. T. Chau, C. C. Chan, and C. Liu, "Overview of permanent-magnet brushless drives for electric and hybrid electric vehicles," *IEEE Transactions on Industrial Electronics*, vol. 55, no. 6, pp. 2246–2257, 2008.

[4] K. W. Lee, D. K. Kim, B. T. Kim, and B. I. Kwon, "A novel starting method of the surface permanent-magnet BLDC motors without position sensor for reciprocating compressor," *IEEE Transactions on Industry Applications*, vol. 44, no. 1, pp. 85–92, 2008.

[5] J. H. R. Bo Long, Shin Teak Lim and K. T. Chong, "Energy-Regenerative Braking Control of Electric Vehicles Using Three-Phase Brushless Direct-Current Motors," *Energies*, vol. 7, pp. 99–114, 2014.

[6] L. Chu, Y.-f. Jia, D.-s. Chen, N. Xu, Y.-w. Wang, X. Tang, and Z. Xu, "Research on Control Strategies of an Open-End Winding Permanent Magnet Synchronous Driving Motor (OW-PMSM)-Equipped Dual Inverter with a Switchable Winding Mode for Electric Vehicles," *Energies*, vol. 10, no. 5, p. 616, 2017.

[7] D. Zorbas, T. Razafindralambo, D. P. P. Luigi, and F. Guerriero, "Energy efficient mobile target tracking using flying drones," *Procedia Computer Science*, vol. 19, no. Ant, pp. 80–87, 2013.

[8] P. Bertoldi and B. Atanasiu, "Electricity consumption and efficiency trends in the enlarged European Union - Status Report 2009," *Institute for Environment and Sustainability*, p. 62, 2009.

[9] J. C. Gamazo-real, E. Vázquez-sánchez, and J. Gómez-gil, "Position and Speed Control of Brushless DC Motors Using Sensorless Techniques and Application Trends," *Department of Signal Theory, Communications and Telematic Engineering, University of Valladolid*, pp. 6909–6913, 2010.

[10] A. Tashakori and M. Ektesabi, "A simple fault tolerant control system for Hall Effect sensors failure of BLDC motor," *Proceedings of the 2013 IEEE 8th Conference on Industrial Electronics and Applications, ICIEA 2013*, pp. 1011–1016, 2013.

[11] G.-A. Capolino and A. Cavagnino, "New Trends in Electrical Machines Technology-Part II," *IEEE Transactions on Industrial Electronics*, vol. 9, no. 61, pp. 4931–4936, 2014.

[12] P. Kshirsagar and R. Krishnan, "High-Efficiency Current Excitation Strategy for Variable-Speed Nonsinusoidal Back-EMF PMSM Machines," *IEEE Transactions on Industry Applications*, vol. 48, no. 6, pp. 1875–1889, 2012.

[13] M. Bertoluzzo, G. Buja, R. K. Keshri, and R. Menis, "Sinusoidal Versus Square-Wave Current Supply of PM Brushless DC Drives : A Convenience Analysis," *IEEE Transactions on Industrial Electronics*, vol. 62, no. 12, pp. 7339–7349, 2015.

[14] J. De Kooning, J. Van De Vyver, B. Meersman, and L. Vandevelde, "Maximum Efficiency Current Waveforms for a PMSM Including Iron Losses and Armature Reaction," *IEEE Transactions on Industry Applications*, vol. 53, no. 4, pp. 3336–3344, 2017.

[15] J. De Viaene, S. Derammelaere, and K. Stockman, "Load angle estimation for dynamic stepping motor motion applications," *Mechatronics*, vol. 53, 2018.

[16] S. Derammelaere, B. Vervisch, J. De Viaene, and K. Stockman, "Sensorless load angle control for two-phase hybrid stepper motors," *Mechatronics*, vol. 43, pp. 6–17, 2017.

[17] J. De Viaene, F. Verbelen, S. Derammelaere, and K. Stockman, "Energy-efficient sensorless load angle control of a BLDC motor using sinusoidal currents," *IET Electric Power Applications*, vol. 12, no. 9, pp. 1378–1389, 2018.

[18] Y. Vanommeslaeghe, J. Denil, J. De Viaene, D. Ceulemans, S. Derammelaere, and P. De Meulenaere, "Leveraging domain knowledge for the efficient design-space exploration of advanced cyber-physical systems," pp. 351–358, Aug 2019.

[19] S. Derammelaere, C. Debruyne, F. De Belie, K. Stockman, and L. Vandevelde, "Load angle estimation for two-phase hybrid stepping motors," *IET Electric Power Applications*, vol. 8, no. 7, pp. 257–266, 2014.

[20] K. Premkumar and B. V. Manikandan, "Adaptive Neuro-Fuzzy Inference System based speed controller for brushless DC motor," *Neurocomputing*, vol. 138, pp. 260–270, 2014.

[21] P. Vas, "Sensorless Vector and Direct Torque Control," *Monographs in Electrical and Electronic Engineering, Oxford University Press, USA*, vol. 1., p. 768, 1998.

[22] S. Derammelaere, M. Haemers, J. De Viaene, F. Verbelen, and K. Stockman, "A quantitative comparison between BLDC , PMSM , Brushed DC and Stepping Motor Technologies," *19th International Conference on Electrical Machines and Systems, ICEMS*, 2016.

[23] F. Verbelen, S. Derammelaere, C. Debruyne, and K. Stockman, "A general model for 6 switch voltage source inverter," *EPE journal*, vol. 27, no. 1, pp. 23–30, 2017.

[24] M. Seilmeier and B. Piepenbreier, "Sensorless Control of PMSM for the whole speed range using Two-Degree-of-Freedom current control

and HF test current injection for low speed range," *IEEE Transactions on Power Electronics*, no. 99, pp. 1–1, 2014.
[25] F. Vanbecelaere, S. Derammelaere, N. Nevaranta, J. De Viaene, F. Verbelen, K. Stockman, and M. Monte, "Online tracking of varying inertia using a sdft approach," *MECHATRONICS*, vol. 68, p. 12, 2020.
[26] R. Delpoux, M. Bodson, and T. Floquet, "Parameter estimation of permanent magnet stepper motors without mechanical sensors," *Control Engineering Practice*, vol. 26, no. 1, pp. 178–187, 2014.
[27] K. Le, H. Hoang, and J. Jeon, "An Advanced Closed-Loop Control to Improve the Performance of Hybrid Stepper Motors," *IEEE Transactions on Power Electronics*, vol. 32, no. 9, pp. 1–1, 2016.
[28] S. Skogetad, "Probably the best simple PID tuning rules in the world," *AIChE Annual meeting, Reno, NV, USA*, no. 0, 2001.
[29] S. S. J. Bernat, "The adaptive speed controller for the BLDC motor using MRAC technique," *The international Federation of Automatic Control, Milano, Italy*, 2011.
[30] K. J. Åström and R. M. Murray, "Frequency Domain Analysis," *Feedback Systems*, pp. 267–292, 2019.
[31] R. Battiti, "First- and second-order methods for learning: Between steepest descent and newton's method," *Neural Computation*, vol. 4, no. 2, pp. 141–166, 1992.
[32] R. Shanmugasundram, K. Muhammad Zakariah, and N. Yadaiah, "Implementation and performance analysis of digital controllers for brushless DC motor drives," *IEEE/ASME Transactions on Mechatronics*, vol. 19, no. 1, 2014.
[33] Y.-L. Hsu, "Adaptive Tracking Control of a PMSM-Toggle System with a Clamping Effect," *International Journal of Mechanical Engineering and Applications*, vol. 4, no. 1, p. 1, 2016.
[34] Y. L. Hsus, M. S. Huang, and R. F. Fung, "Energy-saving trajectory planning for a toggle mechanism driven by a PMSM," *Mechatronics*, vol. 24, no. 1, pp. 23–31, 2014.
[35] N. Van Oosterwyck and F. Vanbecelaere, "Cad enabled trajectory optimization and accurate motion control for repetitive tasks," in *15th IEEE International Conference on Control and Automation*. IEEE, 2019.

IX. Appendix

The topology of the test setup is visualized in Figure 11. A *dSpace MicroAutoBox II* is used to implement the control strategies. The Digital Signal Processing (DSP) unit of the MicroAutoBox II computes the motor control strategy. In the Field-Programmable Gate Array (FPGA), a hysteresis current control algorithm is implemented based on [23]. Further, an IGBT Power Electronics Teaching System of *Semikron* is used to inject the three-phase currents. The load torque profiles are applied by a permanent magnet synchronous motor (*Siemens 1FK7022-5AK21 – Sinamics s120 drive system*).

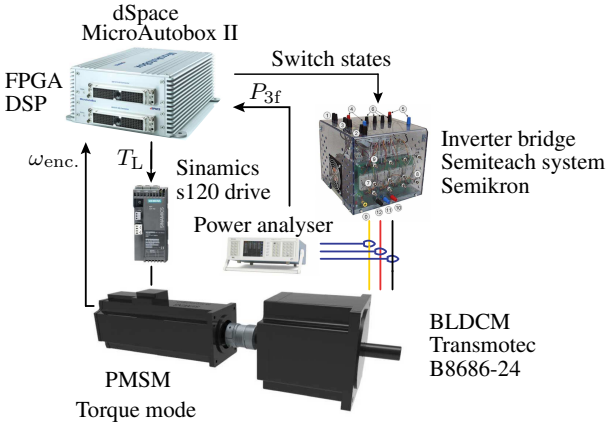

Fig. 11. Test setup used to determine the energy efficiency of the BLDC motor: MicroAutoBox II, Semiteach inverter system Semikron, BLDC motor Transmotec B8686-24, Siemens load motor, power analyser (Tektronix PA4000)

TABLE II
KEY SPECIFICATIONS OF THE 4-POLE THREE-PHASE BLDC MOTOR UNDER TEST, TRANSMOTEC TYPE B8686-24

	Parameter	Value	Unit
P_{nom}	nominal power	225	W
U_{nom}	nominal voltage	24	$\mathrm{V_{dc}}$
n_{nom}	nominal speed	3062	rpm
T_{nom}	nominal torque	0.703	N m
I_{nom}	nominal current	13.76	A
R_{a}	armature resistance	0.07	Ω
L_{a}	armature inductance	0.103	mH
C_{T}	torque constant	0.059	$\mathrm{N\,m\,A^{-1}}$
J_{m}	rotor inertia	800	$\mathrm{g\,cm^2}$

Jasper De Viaene received the Master degree in Industrial Sciences: Electromechanics from the University of Ghent, Belgium in 2015. He received the Ph.D. degree in 2020 at the University of Ghent, Belgium and at the University of Antwerp. He is currently Postdoctoral researcher at University of Ghent and his research interests mainly include advanced and optimal (sensorless) motion control of mechatronic systems driven by fractional horsepower machines.

David Ceulemans received his master's in the industrial sciences: electromechanics: energy at the University of Antwerp, Belgium, in 2018 for his innovations on the hydronic simulation of asphalt solar collectors. Subsequently, he started working as a PhD-researcher within the Constraind Systems Lab (CoSys-Lab) of the Faculty of Applied Engineering at the University of Antwerp, Belgium, where he is currently pursuing his research interests in modeling and controlling energy-efficient applications by researching the control of BLDC and stepper motors.

Stijn Derammelaere was born in Kortrijk, Belgium, in 1984. He received the Master degree in automation from the Tech- nical University College of West-Flanders, Belgium, in 2006. He received the Ph.D. degree in 2013 at Ghent University where he initiated research concerning control engineering, co-design of control and mechatronic systems and the motion control of fractional horsepower machines. He continues this research since 2017 at the University of Antwerp as a professor in mechatronics.

Kurt Stockman received the Industrial Engineer degree from the Provinciale Industriële Hogelschool Kortrijk, in 1994, and the Ph.D. degree from the Katholieke Universiteit Leuven, in 2003. He started his career at the Hogeschool West-Vlaanderen in 1995. He concentrates on the energy efficiency of motor-driven systems and mechatronics systems. Since October 2013, he has been a Professor at Ghent University, Kortrijk, Belgium. His research is characterized by a strong experimental basis and intense collaboration with industry.